American Mineralogist, Volume 72, pages 89–101, 1987

Synchrotron radiation XANES spectroscopy of Ti in minerals: Effects of Ti bonding distances, Ti valence, and site geometry on absorption edge structure

GLENN A. WAYCHUNAS
Center for Materials Research, Stanford University, Stanford, California 94305, U.S.A.

ABSTRACT

The near *K*-edge X-ray absorption spectra of Ti in a suite of silicate and oxide minerals have been examined in an effort to improve Ti characterization in solids. The spectra consist of electronic excitations, occurring in the "pre-edge" region, and multiple scattering resonances on the side and top of the edge. The pre-edge features are insensitive to Ti–O bond length, but are sensitive to valence, occurring about 2.0 eV lower in energy in Ti^{3+} samples. The second pre-edge feature is also sensitive to octahedral site distortion and to the presence of tetrahedral Ti^{4+} owing to intensification created by *d-p* orbital mixing. The multiple scattering features shift to lower energy as Ti–O bond length increases and also change in number, intensity, and energy in response to varying ligand symmetry.

Analysis of these spectral features suggests that tetrahedral Ti^{4+} probably occurs only at very small concentration levels in silicates, even when the total Si^{4+} and Al^{3+} concentration is well below that necessary to fill available tetrahedral sites, as in the melanite-schorlomite garnets. The levels of Ti^{3+} are more difficult to determine because of an apparent sensitivity of the pre-edge Ti^{4+} features to bulk chemistry. However, the overall results are consistent with only small amounts of Ti^{3+}, even in samples from localities where other analyses (wet chemical and Mössbauer) have indicated significant Ti^{3+}.

INTRODUCTION

Ti is an abundant element in the Earth's crust and a major constituent in many minerals. It also occurs as a trace or minor element in many mineral assemblages where knowledge of the site partitioning and site occupations would be of value in geochemical calculations.

Unfortunately, owing to the limitations of most analytical techniques, Ti ordinarily can be studied only in terms of gross abundance as by electron microprobe, or by inference from details of optical spectroscopy and Mössbauer spectroscopy of Fe coexisting in the same mineral. In selected cases, X-ray and neutron structure refinement procedures can be used to determine Ti site occupations. However, these methods do not work well for small Ti concentrations. Wet-chemical analysis has been used, particularly before the advent of electron microprobes, to specify Ti contents in minerals. However, though the overall Ti concentration is probably accurately determined, the fraction of Ti^{3+} obtained in this way may be largely erroneous (Whipple, 1979).

The difficulty of studying Ti stems from its chemical character. It is usually found in the tetravalent state in terrestrial minerals, and in this case has no 3*d* electrons and thus no absorption in the visible spectrum. Charge transfer can occur with nearby Fe^{2+} in a structure, but this does not enable accurate estimation of either Ti concentration or site occupation. The X-ray scattering power of Ti^{4+} is also too similar to Mn, Fe, and other first-row transition metals to allow accurate site-occupancy refinement by X-ray diffraction methods. Thus, the first-row transition elements are commonly lumped together with Ti in crystal-structure refinement. Therefore, Ti has been generally incompletely characterized in most mineral systems.

The main questions concerning the crystal chemistry of Ti in minerals are (1) to what extent it actually enters tetrahedral coordination; (2) its site preference among octahedral sites of varying size, charge balance, and distortion; and (3) the Ti^{3+}/Ti_{tot} ratio. The ionic radius of Ti^{4+} is such (Shannon and Prewitt, 1969) that substitution for Fe^{3+} should occur given suitable charge balancing. Since Fe^{3+} often enters tetrahedral coordination in oxides and silicates, it follows that Ti^{4+} should also replace Si^{4+} when there is a paucity of Si^{4+} for the available tetrahedral sites. One might naively expect that the larger valence of Ti would even favor Ti^{4+} over Fe^{3+} for tetrahedral substitution for Si^{4+}. However, evidence for tetrahedral Ti^{4+} in naturally occurring species is weak or controversial (Hartman, 1969). Even in schorlomite garnets with very large tetrahedral-site Si deficiencies, it appears that Al^{3+} and Fe^{3+} substitute in the Si site in favor of Ti^{4+} despite its abundance (Schwartz et al., 1980; Dowty, 1971; Huggins et al., 1977a).

Ti^{4+} can enter tetrahedral coordination in special cases where Si^{4+}, Al^{3+}, or Fe^{3+} are unavailable in sufficient amounts, such as synthetic cation-excess NiTi spinels

0003–004X/87/0102–0089$02.00

(Lager et al., 1981), where the strong preference of Ni^{2+} for octahedral sites dictates the site partitioning, in synthetic Ti-rich andradite (Weber et al., 1975), and in synthetic (Ca,Y,Fe,Ti) garnets (Geller et al., 1965). These cases suggest that tetrahedral Ti^{4+} can be accommodated in considerable amounts by stable structures. Hence the notion that small fractions of the available Ti^{4+} may reside on tetrahedral sites in natural species cannot be readily dismissed.

In natural pyroxenes, Ti is generally refined on the smaller octahedral M1 site with no clear evidence for any tetrahedral occupancy (Peacor, 1967). Even in cases where considerable Ti^{3+} is present, as in a meteoritic pyroxene (Dowty and Clark, 1973), all Ti appears to reside in M1.

In amphiboles, Ti is usually assigned to the octahedral strip sites M1, M2, and M3, but some investigators have assigned Ti to the tetrahedral sites (Hawthorne, 1981). The best relevant structural refinement is probably the neutron-scattering study of oxykaersutite by Kitamura et al. (1975), who found that Ti is strongly ordered into the M1 site. An earlier X-ray refinement by Kitamura and Tokonami (1971) on the same specimen had refined Fe + Ti together and indicated a preference of these ions for the M1 and M3 sites. In contrast, X-ray refinements of an oxykaersutite by Hawthorne and Grundy (1973) indicated that all of the Ti resided on M2. A refinement by Robinson et al. (1973) also placed all of the Ti in a high-Ti pargasite into M2. Since Ti has a distinctive neutron-scattering amplitude compared with other elements of similar atomic number, neutron-scattering refinements should be superior to X-ray refinements of Ti, given sufficient sample quantities. However, the differences in these refinements may also reflect changes in Ti partitioning during dehydration or oxidation reactions.

In micas, Ti may be a major constituent mainly in the biotites and oxybiotites (Bailey, 1984). X-ray refinements of 1M and $2M_1$ coexisting oxybiotites by Ohta et al. (1982) suggest that Ti preferentially occupies the M2 octahedral site. A study of Ti-bearing synthetic phlogopite solid solutions (Robert, 1976) indicated that Ti solubility increased with increasing temperature and decreased with increasing pressure, and that all Ti substitution occurred on octahedral sites according to the scheme $2Si^{IV} + Mg^{VI} = 2Al^{IV} + Ti^{VI}$. The pressure-temperature behavior is consistent with Ti substitution in a site somewhat smaller than ideal, so that the much smaller tetrahedral site is greatly disfavored. Mansker et al. (1979) have reported considerable Ti (up to 14 wt% TiO_2) in a high-Ba biotite from nephelinite at Oahu, Hawaii. Despite a considerable undersaturation of Si in the tetrahedral site, analysis of chemical-substitution trends favors Ti^{4+} only in octahedral coordination.

The presence of Ti^{3+} is more difficult to pin down. Since Ti usually occurs with Fe^{2+} and Fe^{3+}, the ostensibly unique optical spectrum of Ti^{3+} is likely to be obscured by Fe^{2+}-Ti^{4+} charge transfer (Rossman, 1984; Rossman, 1980; Faye, 1968). Analyses of Ti garnets (Howie and Wooley, 1968; Huggins et al., 1977a, 1977b) generally indicate small amounts of Ti^{3+} and in some cases Ti^{3+}/Ti_{tot} ratios of 25%, but with considerable Fe^{3+} present in most cases. This is in strict conflict with 1-atm aqueous Ti^{3+} chemistry where Ti^{3+} is oxidized to Ti^{4+} by the presence of Fe^{3+}. Oxygen fugacities believed necessary to stabilize Ti^{3+} are too low for terrestrial conditions (Anderson et al., 1970). However, it may be possible that unusually low oxygen fugacities are unnecessary for the stabilization of Ti^{3+} in structures that may preferentially partition Ti^{3+} and isolate it electronically by rapid crystallization. This is by direct analogy to the stabilization of Fe species out of their customary stability ranges by occupation in certain structures (Verhoogen, 1962). Ti^{3+} does occur in major concentrations in lunar and meteoritic minerals.

Another problem is the details of charge-coupled substitutions that must occur in silicates when Ti^{4+} replaces divalent and trivalent ions. For example, in aegirine augites, Ti^{4+} presumably substitutes only for Fe^{3+} and Al^{3+} on the M1 site. Charge balance can be maintained by substitution of Fe^{3+} or Al^{3+} for Si^{4+} on an adjacent tetrahedral site, by vacancies in the M2 sites (one Na vacancy for each M1 Ti^{4+}) or on the M1 sites (one vacancy for three M1 Ti^{4+} ions), or by an excess of Na on the M2 sites such that [Na] > trivalent M1 ions. In pure acmite, only the tetrahedral-substitution or vacancy-generation scheme is possible. In minerals with other structural topologies or more complex chemistry, the possibilities are more numerous and may be quite complicated.

In the present work, the X-ray near *K*-edge absorption specta (XANES) of Ti in a suite of Ti-bearing minerals have been collected in an attempt to correlate structural information on the Ti sites in these species with X-ray absorption spectral features. The XANES region of the absorption spectrum is rich in structure that is sensitive to the details of the Ti coordination environment and the Ti valence (Waychunas et al., 1981). XANES spectroscopy has already proved to be of value in the determination of Fe site occupancies in minerals (Waychunas et al., 1983, 1986), glasses (Brown et al., 1978), and aqueous solutions (Apted et al., 1981, 1985). Ti XANES, in combination with analysis of the extended X-ray absorption fine structure (EXAFS) oscillations, have been used recently to determine the Ti site occupancy in TiO_2-SiO_2 glasses (Greegor et al., 1982) and the coordination of Ti in metamict Ti-bearing oxide minerals (Greegor et al., 1983).

XANES spectroscopy and EXAFS spectroscopy allow a direct probe into the Ti-site environment, unlike most other analytical tools that must be used in an indirect manner. Most importantly, XANES and EXAFS spectra yield information only on a specific ion's immediate environment. Hence there is no averaging of structural information as occurs with X-ray scattering measurements or IR spectroscopy. Further, these techniques can be applied to trace quantities of Ti, given sufficient X-ray flux. On the other hand, XANES spectroscopy suffers from the cur-

Table 1. Ti-bearing samples examined in the investigation

Sample	Source	Chemistry	Reference
Benitoite	San Benito County, California	$Ba_{1.01}Ti_{1.01}Si_{2.98}Na_{0.02}O_{9.00}$; trace Al, Fe, Ca, Sr, Zr, V	Laird and Albee (1972)
Schorlomite garnet*	Magnet Cove, Arkansas (BM 32025a)	$Ca_{2.870}Fe^{2+}_{0.130}(Ti_{0.983}Fe^{2+}_{0.078}Fe^{3+}_{0.728}Mg_{0.152}Mn_{0.040})[Si_{2.352}Al_{0.211}Fe^{3+}_{0.437}]O_{12.000}$	Erickson and Blade (1963)
Schorlomite garnet*	Iivaara, Kuusamo, Finland (BM 50014)	$Ca_{2.833}Na_{0.102}K_{0.022}Fe^{2+}_{0.043}(Ti_{0.908}Fe^{2+}_{0.212}Fe^{3+}_{0.891}Mg_{0.000}Mn_{0.015})[Si_{2.353}Al_{0.305}Fe^{3+}_{0.342}]O_{12.000}$	Lehijärvi (1960)
Schorlomite garnet	Christmas Mountains, Texas (Caltech 8011)	$Ca_{2.925}Fe^{2+}_{0.075}(Zr_{0.165}Hf_{0.006}Ti_{0.815}Fe^{2+}_{0.083}Fe^{3+}_{0.895}Mg_{0.032}Mn_{0.004}Cr_{0.001})[Si_{2.130}Al_{0.356}Fe^{3+}_{0.514}]O_{12.000}$	This study
Melanite garnet	San Benito County, California	$Ca_{3.064}(Ti_{0.672}Fe^{2+}_{0.286}Fe^{3+}_{0.898}Mg_{0.067}Mn_{0.008}Cr_{0.002}Zr_{0.004})[Si_{2.750}Al_{0.189}Fe^{3+}_{0.061}]O_{12.000}$	This study
Neptunite	San Benito County, California (single crystal; Stanford collection)	$Li_{0.600}Na_{2.120}K_{0.920}Ba_{0.010}(Fe_{1.385}Mg_{0.449}Mn_{0.196})Ti_{2.030}Si_{8.030}O_{24.000}$	This study
Titanite	Pale-green crystal (location unknown; Stanford collection)	$Ca_{1.013}(Ti_{0.948}Al_{0.044}Fe_{0.015})[Si_{0.998}Al_{0.002}]O_{5.000}$	This study
Acmitic clinopyroxene	Norway (UCLA collection; MS 2971)	$Na_{0.75}Ca_{0.11}Fe^{2+}_{0.15}(Ti_{0.09}Fe^{3+}_{0.55}Fe^{2+}_{0.10}Mg_{0.06}Al_{0.04}Mn_{0.02})Si_{1.97}O_{6.00}$	W. A. Dollase (UCLA; pers. comm.)
Kaersutite	Hoover Dam, Arizona	$Ca_{1.839}Na_{0.654}K_{0.324}(Ti_{0.634}Fe^{3+}_{0.370}Fe^{2+}_{0.704}Mg_{3.012}Al_{0.603}Mn_{0.010})(OH)_{0.118}F_{0.196}Si_{6.123}Al_{1.877}O_{23.886}$	Campbell and Schenk (1950)
Barkevikite	White Creek, California (UCLA collection; MS 2873)	$Ca_{1.850}Na_{0.769}K_{0.115}(Ti_{0.443}Fe^{3+}_{0.192}Fe^{2+}_{1.730}Mg_{2.465}Al_{0.150}Mn_{0.018})(OH)_{2.27}Si_{5.928}Al_{2.072}O_{22.000}$	This study
Biotite	Molodezhnaya Station, Enderby Land, Antarctica (UCLA collection)	$K_{1.844}Na_{0.029}Ba_{0.009}(Ti_{0.529}Fe^{3+}_{0.348}Fe^{2+}_{2.090}Mg_{2.358}Al_{0.363}Mn_{0.003})Si_{5.317}Al_{2.683}O_{22.000}$	E. S. Grew (pers. comm.)
Ti^{3+} clinopyroxene	G. R. Rossman (California Institute of Technology)	$NaTi^{3+}Si_2O_6$	Prewitt et al. (1972)
Ilmenite**	Hunaker Creek, Yukon Territory, Canada (Stanford collection; 4711)	$FeTiO_3$	This study
Rutile	Macalno, Inyo County, California (Stanford collection; 4839)	$Ti_{0.990}Fe_{0.013}Al_{0.001}Mn_{tr}O_{2.000}$	This study
Anatase	V. T. Baker (analyzed reagent)	TiO_2 with only trace impurities	
αTi_2O_3	ALFA Products, Thiokol, Ventron Division	Ti_2O_3 99.9%	

* Material received as fine powder; quoted analysis is for representative sample from locality. Semiquantitative X-ray fluorescence analysis indicates that these samples have similar concentrations of major ions Ca, Ti, and Fe.

** Fine grains in hematite matrix. Hematite has only trace quantities of Ti.

rent weakness of theory to fully explain spectral features. Hence the analysis approach is at present limited to spectral correlations between standard structures and unknowns.

Most of the data presented in this work have been acquired with the use of synchrotron radiation generated during parasitic storage ring operation at the Stanford Synchrotron Radiation Laboratory (SSRL). In this mode the X-ray flux is sufficient for the acquisition of good-quality XANES data, but problematical for similar-quality EXAFS spectra since the signal to noise requirements for EXAFS are about 20 times higher than those for acceptable XANES. Hence, only the Ti XANES are analyzed in detail here. The quantitative site coordination and bond distances obtainable from high-quality EXAFS spectra will be presented in a future work when dedicated (high-current) beam conditions have been available for the collection of EXAFS data for most samples.

The minerals examined in the present work are summarized in Table 1 along with relevant chemical data.

Experimental procedures

The sample preparation and data collection procedures are identical to those described in Waychunas et al. (1983) except that a helium-filled bag was fashioned around the X-ray beam path to minimize air absorption of the 4.9–5.1-keV radiation. The entrance-beam slits were adjusted to give Ti near-edge structure of about 1.0-eV resolution as judged by pre-edge structure peak widths of anatase run over a range of slit spacings.

Energy calibration on the beam lines at SSRL was done using an iron-foil standard, taking the first inflection point on the *K*-edge as 7111.2 eV. The anatase spectrum was collected repeatedly as

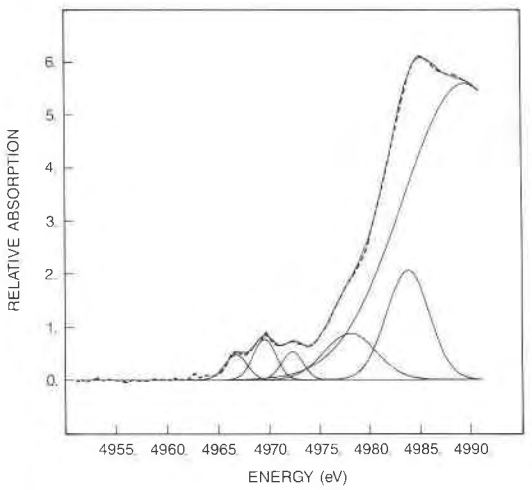

Fig. 1. The near *K*-edge X-ray absorption spectrum of ilmenite fitted with Gaussian features. The dashed line is the observed spectrum. The fit is of representative quality.

an additional standard. This indicated a reproducibility of 0.1 eV in the energy range.

Data analysis for the XANES spectra was accomplished by least-squares fitting of Gaussian distributions to the near-edge spectral envelope after subtraction of the polynomial-fitted photoelectric background absorption. Integrated peak areas are used as a measure of feature intensity. A representative example of such a fit is shown in Figure 1, which depicts the ilmenite near-edge absorption spectrum.

Microprobe analysis of several of the samples was performed on carbon-coated mounted thin sections with a JEOL Model 733 microprobe utilizing the Bence-Albee data-reduction scheme. A beam voltage of 15 kV, current of 15 nA, and diameter of 10 μm was used. The analyses were initially computed taking all Fe as present in the ferrous state. Subsequent recalculation using evaluation of the most probable chemical analysis by the procedure of Dollase and Newman (1984) allowed recasting of the Fe into ferrous and ferric components. For this purpose, all Ti was assumed to be tetravalent.

Results

General near-edge structure

In the silicates and oxides observed, the near-edge X-ray absorption spectra of Ti^{4+} have up to nine resolvable absorption features that can be separated into three subgroups for further discussion. In all of the samples examined in the present study, the Ti occupies mainly octahedrally coordinated sites. The samples most likely to have small amounts of tetrahedral Ti^{4+} or Ti^{3+} are the Ti garnet samples. Thus changes in edge structure are mainly due to variations in octahedral-site geometry.

The edge region under consideration is between 4960 and 5020 eV. Above 5020 eV the features observed are of much reduced amplitude and are generally considered due to single-scattering EXAFS.

The first three features appear in the "pre-edge" region where, in compounds of other transition metals, transitions to unfilled, largely metal character, molecular orbital (MO) levels are observed. These are best exemplified in the anatase and rutile spectra as shown in the comparison of spectra in Figure 2. Of these features, it is the second absorption at about 4969 eV that undergoes the largest intensity change from compound to compound. In the lower-symmetry Ti^{4+} sites, such as in neptunite and kaersutite, this feature is quite strong, whereas the other pre-edge features are weak or absent.

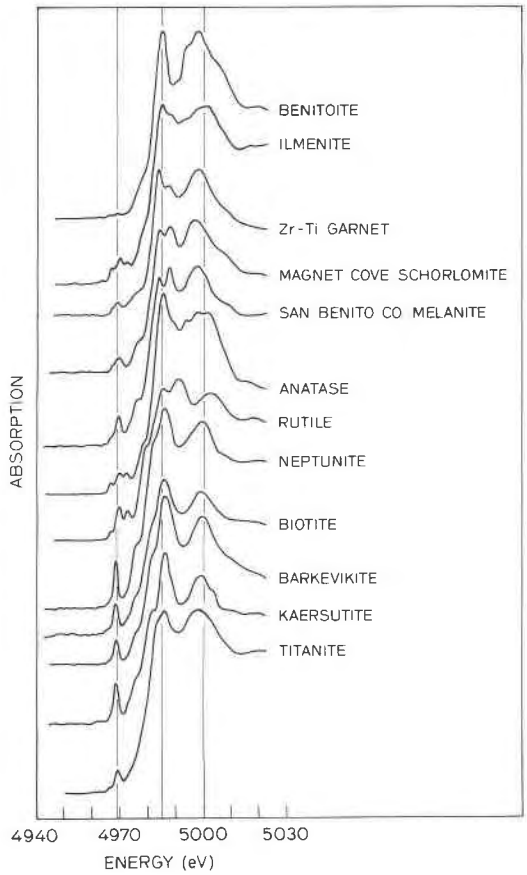

Fig. 2. Comparison plot of near *K*-edge Ti X-ray absorption spectra. The photoelectron background-absorption profile has been removed, and all spectra have been rescaled in amplitude to facilitate comparison.

The existence of three features in the pre-edge region, rather than two as might be expected from straightforward application of crystal-field or MO theory to an octahedral Ti^{4+} bonding arrangement, suggests that a simple one-electron transition interpretation of the Ti edge may be insufficient. The separation of the second and third features is about 2.7 eV in all spectra where these features can be fitted. This is roughly consistent with calculations of the MO levels (Tossell et al., 1974) and the one-electron density of states (DOS) (Grunes et al., 1982) in a TiO_6 cluster. Correlation with the analogous splitting in Ti L-III and O *K* absorption spectra of TiO_2 (Fischer, 1972) is also good. However, the MO calculation reveals no satisfactory unfilled energy level assignable to the first pre-edge feature, and the DOS calculation similarly pre-

Table 2. Energies of fitted Ti X-ray absorption edge features

Sample	Pre-edge features			Main-edge features		
	1	2	3	4	5	6
Benitoite	4966.7(1)	4969.2(1)	*	4978.8(1)	4985.1(1)	*
Schorlomite garnet (Magnet Cove, Arkansas)	4967.1	4969.0	*	4977.2	4983.1	4988.3
Schorlomite garnet (Kuusamo, Finland)	4967.0	4969.0	*	4976.9	4983.1	4988.3
Schorlomite garnet (Christmas Mountains, Texas)	4967.5	4969.3	*	4978.3	4983.5	4988.4
Melanite garnet (San Benito, California)	4966.5	4969.1	*	4976.4	4982.6	4988.1
Neptunite	4966.9	4969.0	*	4975.6	4982.1	4988.0
Titanite	4966.5	4969.3	4973.9	4977.8	4982.0	4986.6
Acmitic clinopyroxene	4966.7	4968.9	4971.5	4977.8	4983.8	4987.5
Kaersutite	4966.6	4968.6	*	4975.4	4981.1	4987.0
Barkevikite	4966.9	4968.7	*	4976.0	4981.6	4987.2
Biotite	4966.3	4968.7	*	4976.5	4983.3	4988.8
$NaTi^{3+}Si_2O_6$	4966.1	4967.3	4969.1	4976.5	4981.9	4987.3
Ilmenite	4966.6	4969.6	4972.1	4978.1	4983.7	4989.2
Rutile	4967.0	4969.7	4972.7	4978.6	4984.2	4993.4
Anatase	4966.7	4969.5	4972.0	4977.8	4984.1	4990.2
αTi_2O_3	*	4967.7	*	4976.0	*	4985.5
Ba_2TiO_4**	*	4967.8	*	4974.0	4979.5	4983.8

* Feature too weak or ill-defined to fit.
** Analysis of spectrum collected by Greegor et al., 1983.

dicts no weak peak in this region. This failure of one-electron theory suggests that the first peak is due to a multielectron excitation process.

Many investigators have observed the first weak pre-edge peak in the rutile absorption spectrum, but they usually do not attempt to assign it to any transition (Fischer, 1972; Balzarotti et al., 1980). However, the second and third features are commonly assigned to the $2t_{2g}$ and $3e_g$ "crystal-field" states, respectively. Differing interpretations for the first peak have been suggested by Grunes (1982), who assigned the weak first feature to a core hole exciton state, and by Greegor et al. (1983) who assigned the first feature to the normally filled $1t_{1g}$ state, which gives rise to an absorption through a shake up or shake off transition during the formation of the core hole.

The next three absorption features occur on the steeply sloped side of the absorption edge and at its first crest. In benitoite, only two of these three features are observed, whereas in the schorlomite-melanite garnets, the edge crest appears to have been split relative to the benitoite edge and the fourth feature shifted to slightly lower energy.

In neptunite and the other silicates where Ti presumably occupies low-symmetry six-coordinated sites, the edges are all similar with two features constituting shoulders on the main edge in addition to a single well-defined edge crest.

These features on the main part of the edge are generally believed to be due to multiple scattering of the ejected photoelectric wave by the atomic cage formed by the first few neighbor atomic shells. As such, their energy and intensity should be sensitive to details of this ligand arrangement (Kutzler et al., 1980). Other interpretations have been made, for example, that of Bair and Goddard (1980), who argued that the first main shoulder on the absorption edge (the fourth feature as defined in this work) is due to a $1s$ to $4p$ plus shake down transition, i.e., a two-electron transition process.

The last three features seen on the Ti edge of the examined species occur about a second major absorption crest at about 4998 eV. In anatase and benitoite, three clear features are evident, but in other samples these appear blurred into a single broadened crest. Since features on this crest are usually not resolved, there was no attempt made to fit them to individual peaks with the least-squares procedure.

The XANES spectrum of Ti^{4+} in tetrahedral coordination in the compound Ba_2TiO_4 (Greegor et al., 1983) was also fitted by the least-squares procedure. In this spectrum only one strong pre-edge feature is observed, and this occurs at somewhat lower energy than the corresponding peak in the octahedral Ti^{4+} spectra. The rest of the edge is similar to that of benitoite, except that there is an additional weak feature on the side of the main edge.

Past results with Fe compounds and minerals (Waychunas et al., 1983) and other transition-metal compounds (Wong et al., 1984; Bianconi et al., 1985) suggest that the edge and pre-edge features yield somewhat differing but complementary information about the absorber site. The energies of the pre-edge features are relatively insensitive to changes in mean metal–oxygen distance, but their intensity is coupled to the degree of d-p mixing which accompanies octahedral-site distortion. Tetrahedral coordination introduces considerable such mixing with dramatic intensification of pre-edge features. In contrast, the features on the main part of the edge may vary markedly in energy with rather subtle changes in the site

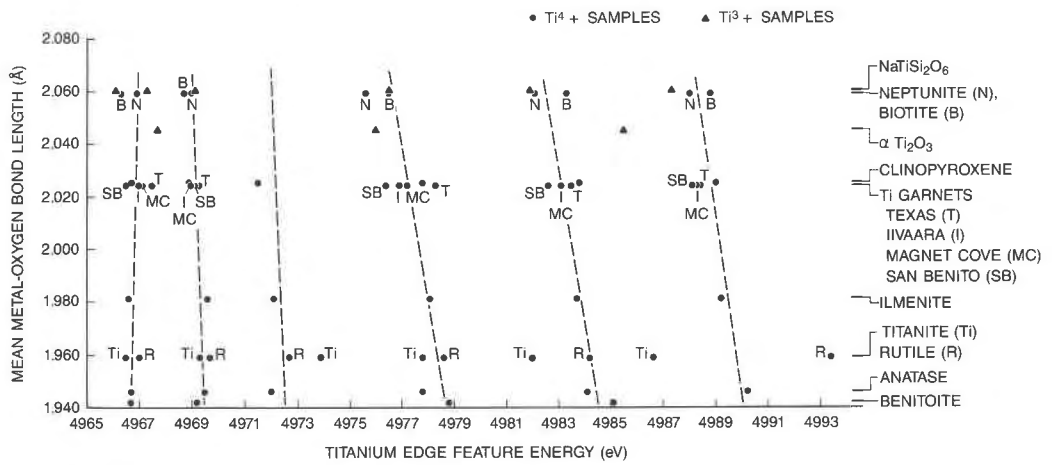

Fig. 3. Effect of mean metal–oxygen bond length on Ti near *K*-edge feature energies.

geometry and are relatively sensitive to the mean metal–oxygen distance. This sensitivity is a consequence of the multiple scattering about the atomic cage that gives rise to these features. The energies of all fitted features in the compounds studied appear in Table 2.

Shifts of XANES feature energies with metal-oxygen bonding distance

The positions of the first six identified pre-edge and main edge features are plotted in Figure 3 as a function of the mean Ti–O distance. Although there is considerable scatter, the trend of decreasing energy with increasing Ti–O distance is clear in the main-edge features. Some of the scatter may be due to the use of inappropriate distances. For example, there is only a relatively small proportion of Ti^{4+} substituting for Fe^{3+} in the clinopyroxene hence, it is not known how closely the Ti site in clinopyroxene is approximated by distances refined on the basis of mainly Fe^{3+} in M1. Given the similarity of Ti^{4+} and Fe^{3+} radii, it is reasonable that these site distances should also be quite similar. The energy shift for the main-edge features is about −20 eV/Å, which is similar to that observed for Fe^{2+} edge features (Waychunas et al., 1983).

The absorption-feature positions for tetrahedral Ti^{4+} in Ba_2TiO_4 do not correspond to the octahedral-feature positions that would be expected for the Ti–O mean distance in Ba_2TiO_4 of 1.74 Å and are more similar to octahedral Ti^{4+} features appropriate to a Ti–O distance of 1.94 Å. This is the effect of the reduced ligand field strength owing to the smaller coordination number and is also observed in Fe^{2+} edge spectra (Waychunas et al., 1983). However, in Fe^{2+} spectra, the main edge-crest energies for the four-coordinated species are at energies higher than any of those observed in six-coordinated Fe^{2+} samples.

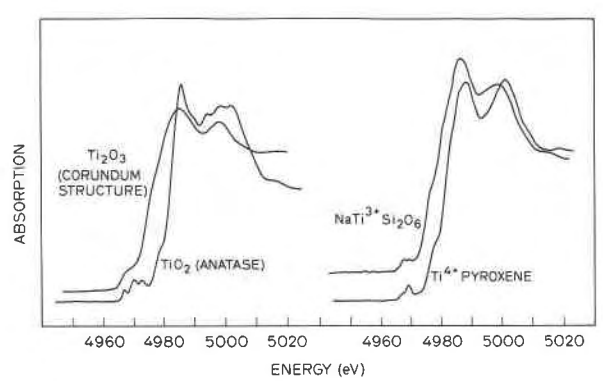

Fig. 4. Comparison of the near *K*-edge spectra of analogous Ti^{3+} and Ti^{4+} structures.

Edge variations between Ti^{4+} and Ti^{3+}

Two samples with high Ti^{3+} concentrations were examined, αTi_2O_3 with the corundum structure (Newnham and DeHaan, 1962), and $NaTiSi_2O_6$ presumed to be isostructural with acmite (Prewitt et al., 1972). The αTi_2O_3 edge was quite smooth with only four resolvable features (Fig. 4). In this respect, the edge is similar to that of Fe in αFe_2O_3 (Calas et al., 1980).

Gaussian line fitting of the αTi_2O_3 edge indicates an energy shift of analogous features relative to the Ti^{4+} samples. The broad pre-edge peak is shifted by −1.8, −1.9, and −2.0 eV relative to the main pre-edge peaks in anatase, ilmenite, and rutile, respectively. Similarly, the side-edge peak fitted at 4976 eV in αTi_2O_3 is shifted −1.8, −2.1, and −2.6 eV relative to these spectra.

The edge-crest energies are not as easily compared because only a single broad feature tops out the αTi_2O_3 edge. However, if the position of this feature is compared with the average position of the edge-crest features on the anatase, ilmenite, and rutile edges, the relative energy shifts observed are −1.7, −1.0, and −3.3 eV, respectively. Thus there is an average shift of about −2.0 eV for each feature or segment of the edge. Examination of Figure 3 reveals that most, if not all, of the shifts in the main-

edge features are due to changes in the Ti–O distance. In contrast, the shift of the pre-edge feature is much larger than any Ti–O bond-length effect.

The $NaTiSi_2O_6$ spectrum is also depicted in Figure 4, where it is compared with that of Ti^{4+} in the clinopyroxene sample. The $NaTiSi_2O_6$ sample consisted of a finely ground powder produced from a small (0.5 mm) single crystal. The best spectra obtained were noisier than those from other samples owing to the small amount of sample. Comparison of the fitted-feature positions with those in the Ti^{4+} clinopyroxene sample gave results in accordance with those observed with the oxide spectra. All three pre-edge features could be fitted and showed energy shifts of -0.6, -1.6, and -2.4 eV; the two side-edge features, -1.3 and -1.9 eV; and the edge crest, -1.7 eV. As with the oxides, the main-edge features appear to be shifted consistent with the change in bond length, whereas the pre-edge features have a much larger valence effect.

Intensity of pre-edge features as a function of site distortion

As noted above, the intensity of the second pre-edge feature on the Ti *K*-edge appears to be sensitive to Ti-site geometry. This is a consequence of the nature of the transition process producing the feature, in this case a core 1*s* to mainly Ti-ion-localized 3*d* t_{2g}-type "crystal-field" state. Such a 1*s* to 3*d* transition is Laporte forbidden for a pure electric dipole interaction, but may be partially allowed by mixing noncentrosymmetric orbital character into the excited state. This can be achieved by static or dynamic symmetry reduction, or by electric quadrupole interactions (Roe et al., 1984). The latter, in fact, give rise to a significant proportion of the analogous pre-edge feature in several Cu compounds (Hahn et al., 1982). However, a correlation can be shown with site distortion from perfect octahedral geometry and the 1*s* to 3*d* intensity in silicates (Fig. 5). In this plot, σ^2 is the variance of the 12 bonding angles in the TiO_6 octahedron (Robinson et al., 1971). The error bars indicate the range of site variances observed for each mineral except in the case of the garnet error bar, which indicates the range of observed 1*s* to 3*d* intensities for all four samples. The Ti-site occupancy results of Kitamura et al. (1975) on oxykaersutite and Ohta et al. (1982) on oxybiotite were used to select the Ti octahedral site in the kaersutite and biotite structures for the variance calculation (Table 3).

Although correlation is evident, it is imperfect probably because orbital mixing is not a simple function of bond-angle variance. In contrast, plots of 1*s* to 3*d* intensity versus bond-length variance show much less correlation. This is as expected, because the radial part of the atomic orbital wave functions is largely unimportant in transition probability (Cotton, 1971). Neither type of plot for the oxides shows much correlation. The pre-edge region in all Ti oxide spectra is different from that of the Ti-containing silicates, suggesting that the factors controlling the pre-edge feature intensity in oxides may be different from those in the silicates.

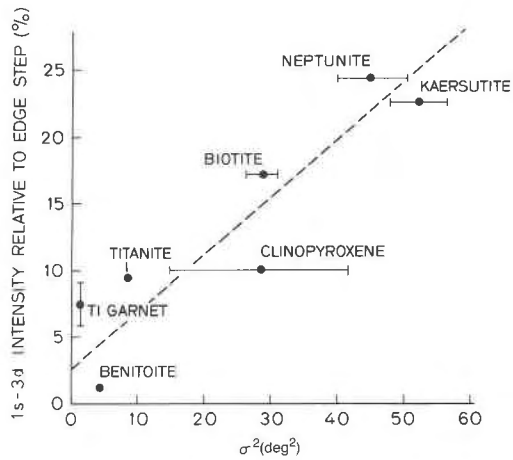

Fig. 5. 1*s* → 3*d* feature intensity as a function of bond-angle variance in octahedral Ti sites in minerals.

Discussion

The concentration of tetrahedral Ti^{4+} in natural silicates

The plot in Figure 5 suggests that the 1*s* to 3*d* intensity observed on the *K* absorption edge in silicates is largely due to distortions in octahedrally coordinated sites, and that it is consistent with the degree of such distortion. Since the presence of a portion of tetrahedral Ti^{4+} would also greatly intensify the 1*s* to 3*d* feature, the presence of tetrahedral Ti^{4+} could be quantitatively estimated if these two 1*s* to 3*d* absorption intensification effects could be separated. The 1*s* to 3*d* absorption in Ba_2TiO_4 is quite strong, being 70% of the intensity of the edge-crest maximum. If it is assumed that the silicate 1*s* to 3*d* feature intensifies in direct proportion to the tetrahedral Ti^{4+} content and that Ba_2TiO_4 is a suitable 100% tetrahedral standard, then rough constraints can be placed on the possible tetrahedral Ti^{4+} concentration in the observed species.

For example, the best candidates for significant amounts of tetrahedral Ti^{4+} are the melanite-schorlomite garnets. The chemical analyses (Table 1) indicate that all have large tetrahedral-site Si deficiencies and high Ti contents, but also have large concentrations of Fe^{3+} that substitute on the tetrahedral sites. The effect of the small andradite structure site distortion is estimated from Figure 5 at 3% of the edge-crest absorption. The observed mean intensity for all four garnet samples is 7.5%.

If one relates the total 1*s* to 3*d* intensity in terms of the octahedral and tetrahedral Ti^{4+} derived intensities using the 3% and 70% intensification factors and the proportions of octahedral and tetrahedral Ti^{4+}, a mean tetrahedral Ti^{4+} concentration of 6.7% of all Ti^{4+} is obtained. The presence of Ti^{3+} is neglected. In each individual case, the respective tetrahedral proportions are San Benito melanite 10.1%, Texas schorlomite 4.1%, Ivaarite schorlomite 6.2%, and Magnet Cove schorlomite 6.2%.

However, other factors can also lead to 1*s* to 3*d* inten-

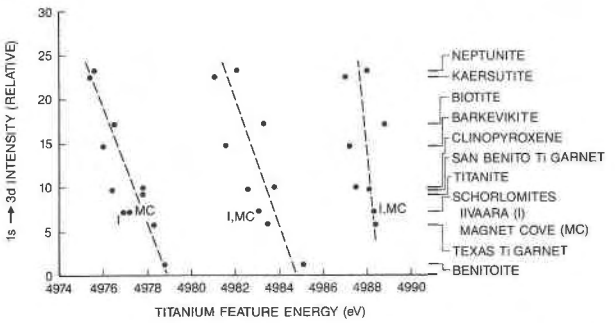

Fig. 6. $1s \rightarrow 3d$ feature intensity as a function of multiple scattering (main-edge) feature energy.

sification. In solid solutions there are always local distortions produced by neighbor-cation substitutions. In the case of the Ti garnets, the new analyses in this study as well as the literature analyses indicate mainly Ca-filled eight-coordinated sites. Because the octahedral sites share edges only with the eight–coordinated sites, the largest geometric effects that would occur from Ca substitution should not be present. However, charge-coupled substitutions such as Fe^{3+} for Si^{4+} in adjacent corner-sharing tetrahedra could have considerable effect. Since the bond-angle variance for the andradite structure refined by Novak and Gibbs (1971) is so small, almost any such variations may increase the site distortion and thus produce greater $1s$ to $3d$ intensity. Hence, the $1s$ to $3d$ intensity observed may not require the presence of any significant amount of tetrahedral Ti^{4+} for its explanation.

Another consideration is any energy shift in the $1s$ to $3d$ transition due to the coordination change from sixfold to fourfold. In Ba_2TiO_4, the $1s$ to $3d$ transition is shifted some 1.6 eV down from its position in the three Ti^{4+} octahedral oxides examined in this study. If a similar shift occurs in the $1s$ to $3d$ absorption in silicates, then one might expect to see an increasingly down-shifted or asymmetric $1s$ to $3d$ peak as the tetrahedral Ti^{4+} content increases. Since the tetrahedral absorption intensity should overwhelm the octahedral intensity for any appreciable amount of tetrahedral Ti^{4+}, and the shift is presumably smaller than the peak width (about 2 eV), a shift rather than a peak shoulder should be seen. Such is not observed, and this is also evidence against significant Ti^{3+} in the garnets, as will be considered below.

Eventually, the clearest distinction between tetrahedral Ti^{4+} and any octahedral Ti^{4+} in a distorted environment must be made with the use of specially characterized standards. For example, Ti XANES and EXAFS spectra should be obtained for Ti-bearing garnets that have had high-quality site-occupancy refinements made with neutron-diffraction methods.

Effect of site symmetry on XANES structure

The spectal sequence depicted in Figure 2 was arranged to suggest a progression in Ti^{4+} edge structure as the site symmetry varies. In benitoite, the Ti site has 32 symmetry with a single Ti–O distance. Accordingly, a single feature is seen on the main edge without subsidiary shoulders. Multiple features are resolved about the second maxima near 4998 eV. The garnet spectra all have similar edges inasmuch as there is no shoulder immediately below the first edge crest, but the main edge has been "split" into two features that vary in relative intensity among the samples. The second major edge maximum is at an energy similar to that in the benitoite spectrum, but has unresolved features. The garnet Ti site symmetry is nominally $\bar{3}$ with a center of symmetry and six equivalent Ti–O distances. However, the garnets in this study are actually solid solutions of several components and have intrinsic site-occupation disorder. Thus, there is actually some range of Ti–O distances and site symmetries. It is thus possible that the "split" edge observed in the garnets is due to symmetry breaking by chemical disorder.

In order to consider this further, the energy of the features on the main-edge maximum (the fourth, fifth, and sixth features depicted in Fig. 3) can be plotted against the $1s$ to $3d$ intensity (Fig. 6). The features generally shift to lower energies, and features five and six progressively separate as the $1s$ to $3d$ intensity increases. The downshift in energy is expected due to the general correlation of site size and distortion in silicates (Goldman and Rossman, ms.). The energies of the benitoite features form a smooth trend with the feature energies of the other samples, suggesting that the fourth and fifth garnet features are the same as those observed on the benitoite edge. These move to lower energies as the site is increasingly distorted, and the sixth feature appears at about 4988 eV. As seen in Figure 2, this new feature increases in intensity with the $1s$ to $3d$ feature. Fitting of these features shows that the increase in the sixth-feature intensity is only a small fraction of the increase in the $1s$ to $3d$ intensity. This is consistent with the sixth feature being a multiple scattering effect as opposed to some type of direct electronic excitation.

The correlation of the $1s$ to $3d$ and sixth-feature intensity demonstrates the effect of distortion on the two differing types of edge features, but does not yield an explanation for its source. This could conceivably be small amounts of tetrahedral Ti^{4+}, but another explanation derives from the chemical analyses. The San Benito melanite has the smallest tetrahedral Si deficiency, but it has the largest $1s$ to $3d$ intensity and largest sixth feature. In contrast, the Texas schorlomite has the largest Si deficiency and the smallest $1s$ to $3d$ intensity and sixth feature. Since one expects Si deficiency to correlate with tetrahedral Ti^{4+} occupancy if the latter occurs at all, these observations suggest that the $1s$ to $3d$ intensity is not due to tetrahedral Ti^{4+}.

A possible factor influencing site distortion may be charge balancing between the octahedral and tetrahedral sites. Ti^{4+} on the octahedral site may force the structure to position a 3+ ion on one of the nearest tetrahedral sites. In the San Benito melanite there are not enough trivalent ions on these tetrahedral sites to locally balance

Table 3. Ti site symmetry, bond length, and bond-angle variance information

Sample	Ti site(s)	Symmetry	Metal–oxygen bond length (Å)			σ^2 (deg^2)	References
Benitoite	One, octahedral	32	6—1.942			4.46	Fischer (1969)
Schorlomite-melanite garnets	One, octahedral	$\bar{3}$	6—2.024*			1.37	Novak and Gibbs (1971)
Neptunite	Two, octahedral	1	2.045 1.918 2.096 2.065 2.218 1.990 2.055**		2.067 2.067 2.195 1.986 2.010 2.057 2.064**	40.0, 50.6	Cannillo et al. (1966)
Titanite	One, octahedral	1	2.014 1.991 1.984 1.973 2.025 1.766 1.959**			8.65	Speer and Gibbs (1976)
Acmitic clinopyroxene	M1, octahedral	2	2—2.109† 2—2.029† 2—1.936† 2.025**			41.9† 14.8††	Clark et al. (1969)
Kaersutite, barkevikite	M1, M2, M3 octahedral	2, 2, 2/*m*	2—2.005 2—2.188 2—1.950 2.047**	2—2.131 2—2.045 2—1.977 2.051**	4—2.089 2—2.001 2.059**	47.9, 31.2, 71.9 56.4, 34.0, 79.4	Hawthorne (1978) Kitamura et al. (1975)
Biotite	M1, M2 octahedral	2/*m*, 2	2—2.142‡ 2—2.088‡ 2—1.947‡ 2.059**		2.137§ 2.142§ 2.091§ 2.091§ 1.950§ 1.947§ 2.060**	31.7, 26.4	Hazen and Burnham (1973) Ohta et al. (1982)
Ilmenite	One, octahedral	3	3—2.0886 3—1.8744 1.9815**			86.0	Wechsler and Prewitt (1984)
Rutile	One, octahedral	*mmm*	2—1.984 4—1.946 1.959**			29.5	Cromer and Herrington (1955)
Anatase	One, octahedral	$\bar{4}2m$	2—1.964 4—1.937 1.946**			107.2	Cromer and Herrington (1955)

* Andradite.
** Mean metal–oxygen distance.
† Acmite.
†† Hedenbergite.
‡ M2 site, 1M structure.
§ 2M$_1$ structure.

the octahedral Ti^{4+}, whereas in the Texas schorlomite there are plenty. The two other schloromite garnets have intermediate situations. The poorer the charge balancing, the more distortion presumably occurs in the octahedral Ti^{4+} site, and thus the larger the 1*s* to 3*d* intensity.

This explanation also involves most of the Ti^{4+} in the garnet structure, whereas the assumption of a small portion of the Ti^{4+} content on the tetrahedral site presumably affects only that fraction. On the basis of charge balance, Ti^{4+} should not prefer tetrahedral sites sharing corners with octahedral sites also containing Ti^{4+}. Thus, any tetrahedral Ti^{4+} would tend not to affect other octahedral Ti^{4+} in the garnet structure. However, owing to the edge-feature energy shifts observed as 1*s* to 3*d* intensity changes, most of the Ti^{4+} in the structure must be affected by a site distortion. This is most consistent with distortion of the octahedral Ti^{4+} sites to similar degrees, rather than tetrahedral occupation by a small fraction of the available Ti^{4+} ions.

The Ti site in ilmenite has site symmetry 3 (Wechsler and Prewitt, 1984), and its absorption spectrum is very similar to the spectra of the garnets, particularly the Texas schorlomite. However, the 1*s* to 3*d* intensity is larger than in the garnet samples. The bond-angle variance of the ilmenite Ti site is 86 deg^2, some 63 times larger than the andradite garnet site. This is due to the loss of the center of symmetry and two considerably differing bond lengths. Nevertheless, it is clear that the 3 and $\bar{3}$ sym-

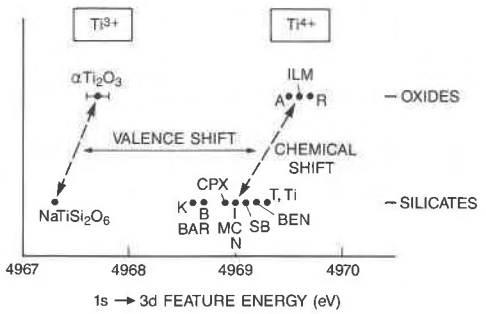

Fig. 7. The energy shift of the $1s \rightarrow 3d$ feature due to valence change between Ti^{3+} and Ti^{4+} and systematic structural and bulk-chemistry differences in oxides and silicates.

metries produce similar multiple-scattering features and that these features may evolve from a simpler set generated by a 32 (benitoite) case.

The other silicates have presumably much-lower symmetry Ti sites, but also fit into the general trends. For example, in the kaersutite edge, the sixth feature has the greatest intensity, and the fifth feature has been reduced to a shoulder. The fourth and fifth features are downshifted in energy relative to the presumed higher-symmetry garnet features.

The biotite, barkevikite, kaersutite, and clinopyroxene edges are all roughly similar with one large main edge absorption feature and two lower energy shoulders on this edge. However, the geometry of the various Ti sites in these species differ considerably, though they are all of similar low symmetry (kaersutite M1, M2, and M3 sites have symmetry 2, 2 and $2/m$, respectively; biotite M1 and M2 sites have symmetry $2/m$ and 2, respectively; M1 site in clinopyroxene has symmetry 2). It thus appears that the edge structure observed on these species may be dependent on the 2 and $2/m$ site symmetry rather than any specific type of site distortion.

The scatter of feature energies is expectable, because multiple-scattering resonances should only change smoothly in energy for smooth variations in atom-cage geometry. Thus, changes as a function of site distortion should be dependent on the initial symmetry as well as the specific type of distortion. The Ti garnet shifts alone are relatively smooth, suggesting that only one type of distortion is occurring as the $1s$ to $3d$ intensity increases.

The anatase edge is interesting because of its unique structure. The Ti site symmetry is $\bar{4}2m$, a highly symmetric site, but the bond-angle variance with respect to an ideal octahedron is 107 deg^2, and the site has no center of symmetry. Despite this, the $1s$ to $3d$ transition is relatively weak, as it is in ilmenite. Given such site distortions and lack of centrosymmetry, it is clear that these oxides must have reduced d-p orbital mixing in the $3d$ MO state relative to the silicates.

The Ti site in rutile differs significantly from anatase and ilmenite, though the $1s$ to $3d$ transition has similar intensity. The Ti site in rutile has mmm symmetry, thus having a center of symmetry, and a bond-angle variance of 29.5 deg^2. The $1s$ to $3d$ intensities in these oxides are thus inconsistent with the results for the silicates, and with symmetry considerations in general. Extension of this study to Ti oxides with lower-symmetry sites and solid solutions may help to explain this anomaly. Ultimately, MO calculations must be performed on model clusters that take into account possible metal–metal bonding and the silicons bonded to coordinated oxygens in the case of silicates.

Identification of Ti^{3+} in silicates

The determination of the Ti^{3+}/Ti_{tot} ratio in silicates from the Ti XANES requires the separation of valence effects from those due to mean Ti–O bond-length, site-symmetry, and bulk-chemistry variations. From an examination of Figure 3, it is clear that the main-edge features (numbers 4, 5, and 6) are largely unaffected by bond length and hence cannot be used to discriminate between long Ti^{4+}–O bonds and short Ti^{3+}–O bonds. However, the pre-edge features, in particular the strong $1s$ to $3d$ absorption, are more affected by valence changes and relatively insensitive to bond length.

In Figure 7 the energies of the Ti^{3+} and nominally Ti^{4+} samples are compared. The mean $1s$ to $3d$ energy for the two Ti^{3+} samples is 4967.5(1) eV, and for the 13 Ti^{4+} samples is 4969.1(1) eV, a shift of 1.6 eV. The oxide $1s$ to $3d$ energies for all samples are larger than the corresponding silicates. This possible chemical effect is 0.4 eV for the Ti^{3+} case and about 0.6 eV for the Ti^{4+} case. It is difficult to select the appropriate set of samples for valence calibration because of this difference between the silicate and oxide samples. There may also be a more subtle shift within the silicate samples owing to the varying nature of the silicate linkages in these samples. For instance, the garnet and titanite energies are similar, and these structures have isolated SiO_4 tetrahedra in their structures. Benitoite has isolated three-member silicate rings and has a $1s$ to $3d$ energy close to the orthosilicates. The energy of the $1s$ to $3d$ feature in the clinopyroxene is somewhat lower than that in the orthosilicates, and it has a chain structure consisting of single-corner-sharing silicate groups. The biotite, kaersutite, and barkevikite features are lower still, and these structures have sheets and double chains of silicate units.

Because of these factors, estimation of the Ti^{3+} content in the samples that are most likely to have finite Ti^{3+} is semiquantitative at best. None of the garnet samples appear to have major Ti^{3+}, although the uncertainties would permit about 10% Ti^{3+}/Ti_{tot}. However, the garnet $1s$ to $3d$ energies do not differ significantly from one another, as might be expected if there were variations in Ti^{3+} content among them. The Mössbauer studies of Schwartz et al. (1980) and Huggins et al. (1977a, 1977b) and the chemical study of Howie and Wooley (1968) suggest that the San Benito garnet specimen may have significant Ti^{3+}, on the order of 20% Ti^{3+}/Ti. However, the particular San

Benito specimen in this study clearly does not have a 1*s* to 3*d* feature position consistent with more Ti^{3+} than the other garnets.

If there is no structural effect on the energy of the 1*s* to 3*d* feature, then the energies of the 1*s* to 3*d* features of the other silicates would suggest definite Ti^{3+} when contrasted to the garnets. However, the presence of any Ti^{3+} in the kaersutite sample, which is strongly oxidized, is quite unlikely. Furthermore, it is most unlikely that the two amphibole samples and the biotite sample selected for this study would all have considerable Ti^{3+} contents. Thus the variations observed are more probably due to structural effects or experimental uncertainties.

EXAFS analysis should aid in the analysis of Ti^{3+} in silicates since the metal–oxygen bond distances should differ by 0.05 to 0.10 Å between the two valence states. However, preliminary analysis of the EXAFS spectra for the Ti garnets in this study does not reveal the presence of significant concentrations of Ti^{3+}.

Conclusions

Analysis of the near-edge features (XANES) in a suite of Ti silicate and oxide minerals indicates the following:

1. The near-edge Ti spectrum is sensitive to site symmetry, and the edge structure differs significantly for markedly differing symmetry. It may be possible to deduce Ti site symmetry solely from near-edge structure, even in the absence of a quantitative theoretical model for the near-edge absorption processes.

2. The multiple-scattering features on the Ti edge are sensitive to Ti–O distances, decreasing in energy as the bond length increases. This verifies trends already observed in other transition-metal compounds.

3. There is no compelling evidence for significant amounts of tetrahedral Ti^{4+} in any of the samples despite relatively high Ti^{4+} concentration in general and substantial Si deficiencies in the garnet samples. The 1*s* to 3*d* intensification that is observed can be explained by charge imbalance–induced octahedral-site distortions.

4. The presence of Ti^{3+} in the silicates examined is possible but difficult to determine unambiguously without standards of similar structure and composition. There is no good evidence for significant Ti^{3+} in the melanite-schorlomite garnets, which are the best candidates of all of the samples for substantial Ti^{3+} content.

5. Relative Ti^{4+} site distortion in the silicates can be judged from the intensity of the 1*s* to 3*d* feature, because the intensity is not usually due to the presence of tetrahedral Ti^{4+}, and from the energy shift of edge features. The energy shift is due to the general trend of larger sites having greater distortion.

6. Variations in the intensity of the $1s \rightarrow 3d$ transition in response to Ti-site symmetry appear to differ between oxides and silicates. This is presumably due to differences in the degree of *p* character orbital mixing into the 3*d* final state, and hence may reflect differing contributions from oxygen 2*p* depending on whether the oxygen is bonded to other metal ions or Si.

7. The shape of the Ti near-edge spectra and the 1*s* to 3*d* feature intensity are consistent with the results of past refinements for Ti site occupation for the kaersutite and biotite samples. However, even given optimal conditions, changes in the site partitioning between octahedral sites of similar symmetry may not affect edge structure in a dramatic enough manner to allow better than qualitative determinations of the partitioning.

Acknowledgments

The author is grateful for assistance with a portion of the data collection at SSRL to Michael Apted, Gordon Brown, Jr., David McKeown, Carl Ponader, and Jason Pressesky. The silicate microprobe analyses were performed by Anne Vaughan. Donations of Ti samples were made by Gordon Brown, Jr., Wayne Dollase, and George Rossman. Reviews by Jack Tossell, Wayne Dollase, and Max Otten improved the quality of the manuscript. Typing and text editing of the manuscript and assembly of the tables were ably performed by Jean King. This work was supported by the NSF-MRL program through the Center for Materials Research at Stanford University. The work at SSRL was supported by the Department of Energy, Office of Basic Energy Sciences; and the National Institute of Health, Biotechnology Resource Program, Division of Research Resources.

References

Anderson, A.T., Jr., Crewe, A.V., Goldsmith, J.R., Moore, P.B., Newton, R.C., Olsen, E.J., Smith, J.V., and Wyllie, P.J. (1970) Petrologic history of Moon suggested by petrography, mineralogy, and crystallography. Science, 167, 587–590.

Apted, M.J., Waychunas, G.A., and Brown, G.E., Jr. (1981) EXAFS study of iron and zinc complexes in hydrothermal solutions. 8th Annual SSRL Users Group Meeting. SSRL report 81-03, 21–22.

——— (1985) Structure and specification of iron complexes in aqueous solutions determined by X-ray absorption spectroscopy. Geochimica et Cosmochimica Acta, 49, 2081–2089.

Bailey, S.W. (1984) Crystal chemistry of the true micas. Mineralogical Society of America Reviews in Mineralogy, 13, 13–60.

Bair, R.A., and Goddard, W.A. (1980) Ab initio studies of the X-ray absorption edge in copper complexes. 1. Atomic Cu^{2+} and $Cu(II)Cl_2$. Physical Review B, 22, 2767–2776.

Balzarotti, A., Comin, F., Incoccia, I., Piacentini, M., Mobilio, S., and Savoia, A. (1980) *K*-edge absorption of titanium in the perovskites $SrTiO_3$, $BaTiO_3$, and TiO_2. Solid State Communications, 35, 145–149.

Bianconi, A., Fritsch, E., Calas, G., and Petiau, J. (1985) X-ray absorption near-edge structure of 3*d* transition elements in tetrahedral coordination: The effect of bond-length variation. Physical Review B, 32, 4292–4295.

Bland, J.A. (1961) The crystal structure of barium orthotitanite, Ba_2TiO_4. Acta Crystallographica, 14, 875–881.

Brown, G.E., Jr., Keefer, K.D., and Fenn, P.M. (1978) Extended X-ray absorption fine structure (EXAFS) study of iron-bearing silicate glasses: Iron coordination environment and oxidation. Geological Society of America Abstracts with Programs, 10, 373.

Calas, G., Levitz, P., Petiau, J., Bondot, P., and Loupias, G. (1980) Etude de l'ordre local autour de fer dans des verres silicates naturels et synthetiques à l'aide de la spectrométrie d'absorption X. Revue de Physique Appliqué, 15, 1161–1167.

Cameron, M., and Papike, J.J. (1980) Crystal chemistry of sili-

cate pyroxenes. Mineralogical Society of America Reviews in Mineralogy, 7, 5–92.
Campbell, I., and Schenk, E.T. (1950) Camptonite dikes near Boulder Dam, Arizona. American Mineralogist, 35, 671–692.
Canillo, E., Mazzi, F., and Rossi, G. (1966) The crystal structure of neptunite. Acta Crystallographica, 21, 200–208.
Clark, J.R., Appleman, D.E., and Papike, J.J. (1969) Crystal-chemical characterization of clinopyroxenes based on eight new structure refinements. Mineralogical Society of America Special Paper 2, 31–50.
Cotton, F.A. (1971) Chemical applications of group theory. Second edition. Wiley, New York.
Cromer, D.T., and Herrington, K. (1955) The structures of anatase and rutile. American Chemical Society Journal, 77, 4708–4709.
Dollase, W.A., and Newman, W.I. (1984) Statistically most probable stoichiometric formulae. American Mineralogist, 69, 553–556.
Dowty, E. (1971) Crystal chemistry of titanium and zirconium garnet: I. Review and spectral studies. American Mineralogist, 56, 1983–2009.
Dowty, E., and Clark, J.R. (1973) Crystal structure refinement and optical properties of a Ti^{3+} fassaite from the Allende meteorite. American Mineralogist, 58, 230–242.
Erickson, R.L., and Blade, I.V. (1963) Geochemistry and petrology of the alkalic igneous complex at Magnet Cove, Arkansas. U.S. Geological Survey Professional Paper 425.
Faye, G.H. (1968) Optical absorption spectra of certain transition metal ions in muscovite, lepidolite, and fuchsite. Canadian Journal of Earth Sciences, 5, 31–38.
Fischer, D.W. (1972) X-ray band spectra and molecular-orbital structure of TiO_2. Physical Review B, 5, 4219–4226.
Fischer, K. (1969) Verfeinerung der Kristallstruktur von Benitoit $BaTi[Si_3O_9]$. Zeitschrift für Kristallographie, 129, 222–243.
Geller, S., Sherwood, R.C., Espinosa, G.P., and Williams, H.J. (1965) Substitution of Ti^{4+}, Cr^{3+}, and Ru^{4+} ions in yttrium iron garnet. Journal of Applied Physics, 36, 321.
Greegor, R.B., Lytle, F.W., Ewing, R.C., and Haaker, R.F. (1982) Investigation of titanium in metamict Nb-Ta-Ti oxides using the extended X-ray absorption fine structure technique. In W. Lutze, Ed. Scientific basis for radioactive waste management, V. Elsevier, Amsterdam.
Greegor, R.B., Lytle, F.W., Sandstrom, D.R., Wong, J., and Schultz, P. (1983) Investigation of TiO_2-SiO_2 glasses by X-ray absorption spectroscopy. Journal of Noncrystalline Solids, 55, 27–43.
Grunes, L.A. (1982) A study of core excitation spectra in 3*d* transition metals and oxides by electron energy loss spectroscopy and X-ray absorption spectroscopy. Ph.D. thesis, Cornell University, Ithaca, New York.
Grunes, L.A., Leapman, R.D., Wilker, C.M., Hoffman, R., and Kunz, A.D. (1982) Oxygen *K* near-edge fine structure: An electron energy loss investigation with comparisons to new theory for selected 3*d* transition metal oxides. Physical Review B, 25, 7157–7173.
Hahn, J.E., Scott, R.A., Hodgson, K.O., Doniach, S., Desjardins, S.R., and Solomon, E.I. (1982) Observation of an electric quadrupole transition in the X-ray absorption spectrum of a Cu(II) complex. Chemical Physics Letters, 88, 595–598.
Hartman, P. (1969) Can Ti^{4+} replace Si^{4+} in silicates? Mineralogical Magazine, 37, 366–369.
Hawthorne, F.C. (1978) The crystal chemistry of the amphiboles. VI. The stereochemistry of the octahedral strip. Canadian Mineralogist, 16, 37–52.
——— (1981) Crystal chemistry of the amphiboles. Mineralogical Society of America Reviews in Mineralogy, 9A, 1–102.
Hawthorne, F.C., and Grundy, H.D. (1973) The crystal chemistry of the amphiboles. II. Refinement of the crystal structure of oxy-kaersutite. Mineralogical Magazine, 39, 390–400.
Hazen, R.M., and Burnham, C.W. (1973) The crystal structure of one layer phlogopite and annite. American Mineralogist, 58, 889–900.
Howie, R.A., and Wooley, A.R. (1968) The role of titanium and the effect of TiO_2 on the cell-size, refractive index, and specific gravity in the andradite-melanite-schorlomite series. Mineralogical Magazine, 36, 775–790.
Huggins, F.E., Virgo, D., and Huckenholz, H.G. (1977a) Titanium-containing silicate garnets. I. The distribution of Al, Fe^{3+}, and Ti^{4+} between octahedral and tetrahedral sites. American Mineralogist, 62, 475–490.
——— (1977b) Titanium-containing silicate garnets. II. The crystal chemistry of melanites and schorlomites. American Mineralogist, 62, 646–665.
Kitamura, M., and Tokonami, M. (1971) The crystal structure of kaersutite. Tohoku University Science Reports, ser. 3, 11, 125–141.
Kitamura, M., Tokonami, M., and Morimoto, N. (1975) Distribution of titanium atoms in oxy-kaersutite. Contributions to Mineralogy and Petrology, 51, 167–172.
Kutzler, F.W., Natoli, C.R., Misemer, D.K., Doniach, S., and Hodgson, K.O. (1980) Use of one electron theory for the interpretation of near edge structure in *K*-shell X-ray absorption spectra of transition metal complexes. Journal of Chemical Physics, 73, 3274–3288.
Lager, G.A., Armbruster, T., Ross, F.K., Rotella, F.J., and Jorgenson, J.D. (1981) Neutron powder diffraction study of defect spinel structures: Tetrahedrally coordinated Ti^{4+} in $Ni_{2.62}Ti_{0.69}O_4$ and $Ni_{2.42}Ti_{0.74}Si_{0.05}O_4$. Journal of Applied Crystallography, 14, 261–264.
Laird, J., and Albee, A.L. (1972) Chemical composition and physical, optical and structural properties of benitoite, neptunite and joaquinite. American Mineralogist, 57, 85–102.
Lehijarvi, M. (1960) The alkaline district of Iivaara, Kuusamo, Finland. Geologinen Tutkimuslaitos (Bulletin de la Commission Géologique de Finlande) no. 185.
Mansker, W.L., Ewing, R.C., and Keil, K. (1979) Barian-titanian biotites in nephelinites from Oahu, Hawaii. American Mineralogist, 64, 156–159.
Newnham, R.E., and DeHaan, Y.M. (1962) Refinement of the αAl_2O_3, Ti_2O_3, V_2O_3 and Cr_2O_3 structures. Zeitschrift für Kristallographie, 117, 235–237.
Novak, G.A., and Gibbs, G.V. (1971) The crystal chemistry of the silicate garnets. American Mineralogist, 56, 791–825.
Ohta, T., Takeda, H., and Takeuchi, Y. (1982) Mica polytypism: Similarities in the crystal structures of coexisting 1M and $2M_1$ oxybiotite. American Mineralogist, 67, 298–310.
Peacor, D.R. (1967) Refinement of the crystal structure of a pyroxene of formula M_IM_{II} $(Si_{1.5}Al_{0.5})O_6$. American Mineralogist, 52, 31–41.
Prewitt, C.T., Shannon, R.D., and White, W.B. (1972) Synthesis of a pyroxene containing trivalent titanium. Contributions to Mineralogy and Petrology, 35, 77–82.
Robert, J.-L. (1976) Titanium solubility in synthetic phlogopite solid solutions. Chemical Geology, 17, 213–227.
Robinson, K., Gibbs, G.V., and Ribbe, P.H. (1971) Quadratic elongation: A quantitative measure of distortion in coordination polyhedra. Science, 172, 567–570.
Robinson, K., Gibbs, G.V., Ribbe, P.H., and Hall, M.R. (1973) Cation distribution in three hornblendes. American Journal of Science, 273A, 522–535.
Roe, A.L., Schneider, D.J., Mayer, R.J., Pyrz, J.W., Widom, J., and Que, L., Jr. (1984) X-ray absorption spectroscopy of iron-tyrosinate proteins. American Chemical Society Journal, 106, 1676–1681.
Rossman, G.R. (1980) Pyroxene spectroscopy. Mineralogical Society of America Reviews in Mineralogy, 7, 93–115.
——— (1984) Spectroscopy of micas. Mineralogical Society of America Reviews in Mineralogy, 13, 145–181.
Schwartz, K.B., Nolet, D.A., and Burns, R.G. (1980) Mössbauer spectroscopy and crystal chemistry of natural Fe-Ti garnets. American Mineralogist, 65, 142–153.
Shannon, R.D., and Prewitt, C.T. (1969) Effective ionic radii in oxides and fluorides. Acta Crystallographica, B25, 925–946.
Speer, J.A., and Gibbs, G.V. (1976) The crystal structure of syn-

thetic titanite, $CaTiOSiO_4$, and the domain texture of natural titanites. American Mineralogist, 61, 238–247.

Tossell, J.A., Vaughan, D.J., and Johnson, K.H. (1974) The electronic structure of rutile, wüstite, and hematite from molecular orbital calculations. American Mineralogist, 59, 319–334.

Verhoogen, J. (1962) Distribution of titanium between silicates and oxides in igneous rocks. American Journal of Science, 260, 211–220.

Waychunas, G.A., Apted, M.J., and Brown, G.E., Jr. (1981) Coordination and valence of Ti in kaersutite, schorlomite, titanite and titanite glass from X-ray absorption spectroscopy. Geological Society of America Abstracts with Programs, 13, 577.

——— (1983) X-ray *K*-edge absorption spectra of Fe mineral and model compounds: Near-edge structure. Physics and Chemistry of Minerals, 10, 1–9.

Waychunas, G.A., Brown, G.E., Jr., and Apted, M.J. (1986) X-ray *K*-edge absorption spectra of Fe minerals and model compounds: II. EXAFS. Physics and Chemistry of Minerals, 12, 31–47.

Weber, H.P., Virgo, D., and Huggins, F.E. (1975) A neutron diffraction and ^{57}Fe Mössbauer study of a synthetic Ti-rich garnet. Carnegie Institution of Washington Year Book 74, 575–579.

Wechsler, B.A., and Prewitt, C.T. (1984) Crystal structure of ilmenite ($FeTiO_3$) at high temperature and high pressure. American Mineralogist, 69, 176–185.

Whipple, E.R. (1979) Errors in chemical analyses of two titanian micas. Amerian Mineralogist, 64, 1311.

Wong, J., Lytle, F.W., Messmer, R.P., and Maylotte, D.H. (1984) A study of the *K*-edge absorption spectra of selected vanadium compounds. Physical Review B, 30, 5596–5610.

MANUSCRIPT RECEIVED MARCH 23, 1986
MANUSCRIPT ACCEPTED SEPTEMBER 2, 1986